Acta Crystallographica Section D
Biological Crystallography
ISSN 0907-4449

Structure determination by multiwavelength anomalous diffraction of aclacinomycin oxidoreductase: indications of multidomain pseudomerohedral twinning

Azmiri Sultana,[a] Igor Alexeev,[b] Inari Kursula,[a] Pekka Mäntsälä,[b] Jarmo Niemi[b] and Gunter Schneider[a]*

[a]Department of Medical Biochemistry and Biophysics, Karolinska Institutet, S-171 77 Stockholm, Sweden, and [b]Department of Biochemistry and Food Chemistry, University of Turku, FIN-20014 Turku, Finland

Correspondence e-mail: gunter.schneider@ki.se

Received 1 September 2006
Accepted 23 October 2006

PDB Reference: aclacinomycin oxidoreductase, 2ipi, r2ipisf.

The crystal structure of aclacinomycin oxidoreductase (AknOx), a tailoring enzyme involved in the biosynthesis of the polyketide antibiotic aclacinomycin, was determined to 1.65 Å resolution by multiwavelength anomalous diffraction using data from selenomethionine-substituted crystals. The crystals belong to space group $P2_1$, with unit-cell parameters a = 68.2, b = 264.5, c = 68.2 Å, β = 119°. Analysis of the intensity statistics clearly showed the presence of pseudomerohedral twinning. The data set could also be indexed and scaled with an $R_{\rm sym}$ of 0.072 in the orthorhombic space group $C222_1$ (unit-cell parameters a = 69.7, b = 117.5, c = 264.4 Å), indicating the possibility of pseudomerohedral twinning along the diagonal between the monoclinic a and c directions. Refinement using this twin operator resulted in an $R_{\rm free}$ of 24.2%. A monoclinic lattice with $a = c$ and β close to 120° can emulate a hexagonal metric, with the possibility of a threefold twin operator along the b axis and three twin domains. Refinement assuming three-domain twinning gave a final $R_{\rm free}$ of 26.5%. The structure of AknOx can be thus refined with comparable $R_{\rm free}$ values using either of the twin operators separately, suggesting the possibility that crystals of AknOx contain six twin domains generated by the twofold and threefold twin operators perpendicular to each other. Both twin operators coincide with noncrystallographic symmetry axes that may promote twinning.

1. Introduction

Twinning is regarded as a defect in crystal growth which often has severe consequences for structure determination and refinement. Crystal twinning has been classified into several different categories. In the case of merohedral twinning, the lattices of two or more distinct domains coincide exactly in three dimensions. In protein crystals, merohedral twinning has been observed as hemihedral (two domains) and tetartohedral (four domains) twinning and the diffraction pattern is a superimposition of the pattern of the two or four separate twin domains (Chandra *et al.*, 1999; Lietzke *et al.*, 1996; Liang *et al.*, 1996; Rudolph *et al.*, 2003; Barends *et al.*, 2005; Yeates, 1997; Yeates & Fam, 1999; Dauter, 2003). In the case of hemihedral twinning, each measured reflection is therefore a weighted sum of the intensities of two reflections, $I(\mathbf{h}_1)$ and $I(\mathbf{h}_2)$, from each of the domains,

$$I_{\rm obs}(\mathbf{h}_1) = (1-\alpha)I(\mathbf{h}_1) + \alpha I(\mathbf{h}_2),$$
$$I_{\rm obs}(\mathbf{h}_2) = \alpha I(\mathbf{h}_1) + (1-\alpha)I(\mathbf{h}_2).$$

Here, α is termed the twinning fraction and represents the fractional volume of the specimen occupied by the domains in

the second orientation. A value of α of 0 or 0.5 corresponds to untwinned and perfectly twinned crystals, respectively. In the case of partial twinning, α can vary between 0 and 0.5. The additional symmetry in merohedral twins is not part of the Laue symmetry group of the crystal, but is a symmetry operator of an apparent higher Laue group of the same crystal system. Twinning of this kind is thus observed in tetragonal, trigonal, hexagonal and cubic crystal systems (Dauter, 2003; Rudolph *et al.*, 2004; Yeates, 1997).

In lower point groups, pseudomerohedral twinning can occur provided it is supported by fortuitous unit-cell geometry. In protein crystallography, this form of twinning has been found in monoclinic and orthorhombic space groups. For instance, an orthorhombic space group with $a = b$ can mimic a tetragonal space group (Frazao *et al.*, 1999). In a monoclinic system, an orthorhombic lattice metric can be emulated under several conditions such as (i) $a = c$ (Ban *et al.*, 1999; Yang *et al.*, 2000; Ito *et al.*, 1995), (ii) the β angle being close to 90° (Larsen *et al.*, 2002; Barends & Dijkstra, 2003) and (iii) when the unit-cell parameters satisfy the condition $c\cos\beta = -a/2$ (Declercq & Evrard, 2001; Rudolph *et al.*, 2004). In the latter case, the two monoclinic cells of the twin domains share the same *a* and *b* axes with opposite directions and can be superimposed by a twofold rotation along an axis perpendicular to the *a* and *b* axes (along *c** of the monoclinic cell). Twinning in pseudomerohedral crystals results from an unfortunate (for the protein crystallographer) coincidence of unit-cell parameters and overlap of the twin domains may not necessarily be optimal. This can sometimes result in a split of reflections, in particular at high resolution (Larsen *et al.*, 2002).

A special case of type (iii) pseudomerohedral twinning can occur in a monoclinic cell with $a = c$ and β approximately 120°, which can emulate a hexagonal metric. The twinned crystal contains three components instead of two and the domains are therefore related by two twinning fractions (α_1 and α_2). This type of crystal has been referred to as *Drilling* (German for tripling; Sheldrick, 1997). To the best of our knowledge, only small-molecule crystals have been found with this kind of twinning (Langer *et al.*, 2004) and no protein crystals of this type have been reported to date.

In the course of our work on the structural enzymology of the biosynthesis of aromatic polyketides (Schneider, 2005), we have crystallized recombinant FAD-dependent aclacinomycin oxidoreductase (AknOx) from *Streptomyces galileus*. This enzyme is involved in the modification of the terminal sugar moiety of aclacinomycins. In a two-step reaction, the enzyme converts rhodinose *via* cinerulose A to L-aculose. In this paper, we report the crystallization of AknOx and the detection and analysis of pseudomerohedral twinning in these crystals. Analysis of the intensity statistics from crystals of AknOx clearly indicated pseudomerohedral twinning. In spite of the presence of multidomain twinning, the structure of AknOx could be determined by multiwavelength anomalous diffraction (MAD). Refinement suggested the presence of six-domain twinning, with a twofold rotation about the axis diagonal between the monoclinic *a* and *c* directions and a threefold twin operator parallel to the *b* axis. The crystals of AknOx are the first protein crystals to show this type of multidomain twinning.

2. Materials and methods

2.1. Protein production and purification

The AknOx gene was amplified from DNA of a lambda clone λ*acm*15 containing part of the *S. galilaeus* ATCC 31615 aclacinomycin biosynthetic cluster (Räty *et al.*, 2002) with PCR primers 5′-TGGGAATTCGACGGTGGCGCGTGCGGCG-3′ (forward) and 5′-TTTAAGCTTCCGGTCAGCCGGGCG-GCC-3′ (reverse). The pBAD/HisB vector (Invitrogen) was modified by replacing the affinity-tag segment between its *Nco*I and *Bgl*II sites with a shorter heptahistidine tag as described in Kallio *et al.* (2006). As a result, the expressed protein contains 19 additional amino acids (MAHHHHH-HHRSAAGTIWEF) at its N-terminus. The PCR product was subcloned as an *Eco*RI–*Hin*dIII fragment, yielding the plasmid pBadhisAknOx, and the correct sequence of the AknOx gene was confirmed by DNA sequencing.

AknOx was produced in *Escherichia coli* TOP10 (Invitrogen) as a fusion protein in 5 l of 2×YT medium at 291 K with 350 rev min^{-1} shaking during 16 h and induced with 200 mg l^{-1} L-arabinose. The protein was routinely purified to homogeneity by Ni^{2+}-affinity chromatography and gel filtration. When necessary, an additional anion-exchange chromatography step was used for further purification. The purity of the protein was verified using SDS–PAGE. Enzymatic activity was confirmed by an *in vitro* assay (manuscript in preparation).

For preparation of selenomethionine-substituted AknOx, the *E. coli* TOP10/pBadhisAknOx glycerol stock was used to inoculate 200 ml chemically defined medium in five 2 l Erlenmeyer flasks. The medium contained 0.8 g l^{-1} L-serine, 0.8 g l^{-1} L-threonine, 0.3 g l^{-1} L-valine, 0.03 g l^{-1} L-tyrosine, 0.04 g l^{-1} L-tryptophan, 0.2 g l^{-1} all other amino acids except methionine, 2 m*M* $MgSO_4$, 0.1 m*M* $CaCl_2$, 0.4% glycerol and M9 salts. After 12 h pre-incubation, 1 mg L-methionine was added to each flask and the cells were allowed to grow until a plateau in optical density (OD_{600}) was reached. At this point, 10 mg selenomethionine was added as powder to each flask and protein production was induced using 3.8 g l^{-1} of L-arabinose. Both pre-incubation and incubation steps were performed at 310 K and 300 rev min^{-1} shaking. The cells were harvested 18 h after induction. Degassed and nitrogenated buffers containing 2 m*M* DL-dithiothreitol were used for subsequent protein purification.

2.2. Crystallization of AknOx

AknOx was crystallized in the presence of the substrate aclacinomycin A (AclA). The diluted protein sample was incubated with a tenfold excess of AclA on ice for 1 h and the solution was then concentrated to final protein (10 mg ml^{-1}) and substrate (2 m*M*) concentrations for crystallization trials. Initial crystallization screening using the hanging-drop vapour-diffusion technique was carried out with a variety of

Table 1
Statistics of data processing.

Values in parentheses are for the highest resolution shell.

	Native AknOx		SeMet		
	2 Å resolution	1.65 Å resolution	Peak	Inflection	Remote
Beamline	X11, EMBL/DESY	BW7B, EMBL/DESY	BW7A, EMBL/DESY		
Wavelength (Å)	0.8138	0.8423	0.9793	0.9797	0.9392
Resolution (Å)	19.87–2.05 (2.14–2.05)	20.0–1.65 (1.7–1.65)	20.0–2.7 (2.80–2.70)	20.0–2.7 (2.80–2.70)	20.0–2.7 (2.80–2.70)
No. of observations	527713	898830	460746	461173	464182
No. of unique reflections	131436	246742	113843	113978	114279
Space group	$P2_1$	$P2_1$	$P2_1$		
Unit-cell parameters					
a (Å)	68.2	68.5	68.2		
b (Å)	264.5	266.2	264.3		
c (Å)	68.2	68.7	68.1		
β (°)	118.7	119.0	118.7		
R_{sym}† (%)	5.2 (15.1)	8.1 (37.1)	6.4 (15.2)	6.4 (15.2)	8.9 (27.4)
Completeness (%)	99.4 (98.7)	95.9 (57.3)	99.5 (99.8)	99.3 (99.7)	99.3 (99.4)
Mean $I/\sigma(I)$	19.4 (8.9)	11.5 (3.4)	17.8 (8.9)	17.9 (8.8)	13.1 (4.9)
Mosaicity (°)	0.10	0.40	0.20	0.20	0.20
Wilson B factor (Å^2)	27.3	22.3	25.0	25.5	27.6
Redundancy	4.0	3.6	4.0	4.0	4.0

† $R_{sym} = \sum_{hkl}\sum_i |I_i - \langle I\rangle| / \sum_{hkl}\sum_i \langle I\rangle$, where I_i is the intensity measurement for a reflection and $\langle I\rangle$ is the mean value for this reflection.

commercial screens from Hampton Research (Crystal Screens I and II, PEG/Ion Screen and IndexHT Screen) and Molecular Dimensions (PACT Screen). 4 µl droplets containing equal volumes of protein solution and mother liquor were allowed to equilibrate against 1 ml reservoir solution. Trigonal-shaped rod-like crystals were grown from several conditions containing polyethylene glycol (PEG) 3350 and various ammonium salts, but diffraction patterns from this crystal form could not be indexed owing to the superposition of several crystal lattices. Yellow rectangular crystals (Fig. 1*a*) were obtained at room temperature using 20%(*w*/*v*) PEG 6000, 0.2 *M* ammonium chloride and 0.1 *M* Tris pH 8.0 as

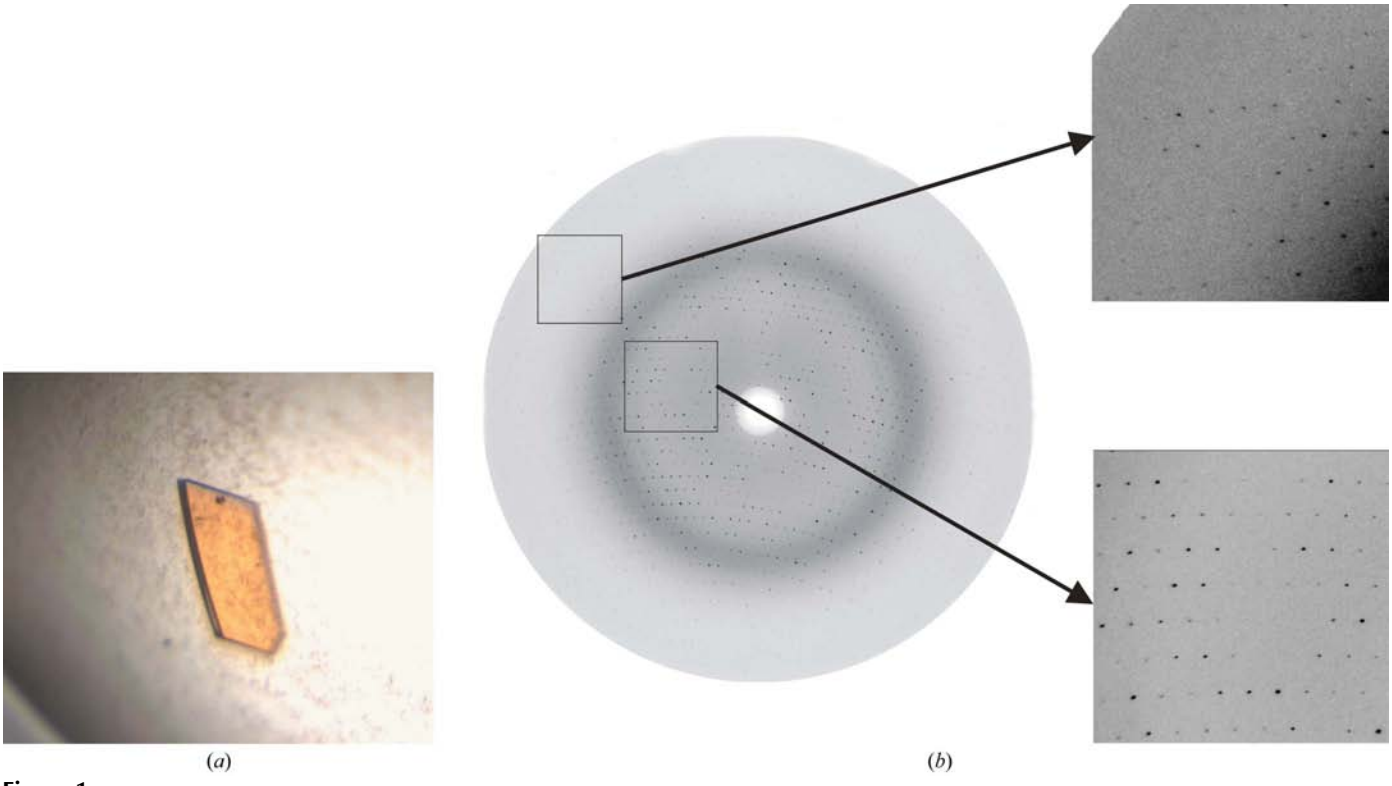

Figure 1
Crystal and diffraction pattern of AknOx. (*a*) Crystal of native FAD containing AknOx cocrystallized with the substrate aclacinomycin A. The longest crystal dimension is approximately 0.3 mm. (*b*) Diffraction image from a native AknOx crystal. The two boxes highlight medium-resolution and high-resolution parts of the image. The resolution at the edge of the detector is 2.05 Å.

mother liquor after approximately three weeks. These crystals were used for data collection and structure determination.

Crystals of the selenomethionine-substituted protein were obtained using the same crystallization conditions. However, microseeding with native crystals as well as the addition of 5 m*M* flavin adenine dinucleotide (FAD) to the protein solution were needed in order to obtain good-quality crystals.

2.3. Data collection and processing

Two data sets from native AknOx crystals were collected to 2.0 and 1.65 Å resolution at beamline X11 using a MAR CCD detector and beamline BW7B using a MAR 345 image plate, respectively, at the EMBL Hamburg Outstation at DESY. Prior to data collection, the crystals were soaked in 25%(*v*/*v*) ethylene glycol mixed with mother liquor for approximately 1 min and flash-frozen in the cryostream at 100 K. An oscillation angle of 0.1° was used for both data sets. Visual inspection of the diffraction images did not show any split reflections either for the high-resolution or low-resolution parts of the images (Fig. 1*b*).

Three data sets at different wavelengths were collected to 2.7 Å resolution from a crystal of selenomethionine-substituted AknOx at beamline BW7A at EMBL/DESY, Hamburg for a MAD experiment. The crystal was flash-frozen using the same protocol as for the native crystals. The peak wavelength for selenium was determined by a fluorescence scan at the beamline. All data sets were processed using the *XDS* program package (Kabsch, 1993) and the *XDSi* interface (Kursula, 2004). Details of the data-processing statistics from crystals of both native and selenomethionine-substituted AknOx are shown in Table 1.

2.4. Detection and analysis of twinning in the crystal

Twinning was first suggested from the analysis of the intensity statistics provided by *XDS* (Kabsch, 1993). The cumulative intensity distribution and second intensity moments were then calculated using the program *TRUNCATE* from the *CCP*4 program suite (Collaborative Computational Project, Number 4, 1994). The local intensity statistics (Padilla & Yeates, 2003) were analyzed using *DATAMAN* (Kleywegt & Jones, 1996). The twinning fraction was initially estimated from the cumulative distribution of *H* (Yeates, 1988) and Britton plots (Fisher & Sweet, 1980) with the *CCP*4 program *DETWIN* (Collaborative Computational Project, 1994) and subsequently refined with the program *SHELXL* (Sheldrick & Schneider, 1997). The self-rotation function calculations were carried out with *MOLREP* (Vagin & Teplyakov, 1997). Native Patterson maps did not contain any significant peaks that might have indicated the presence of pseudo-translation.

2.5. Structure determination, model building and refinement

The selenium sites were located from the MAD data sets with the program *SOLVE* (Terwilliger & Berendzen, 1999)

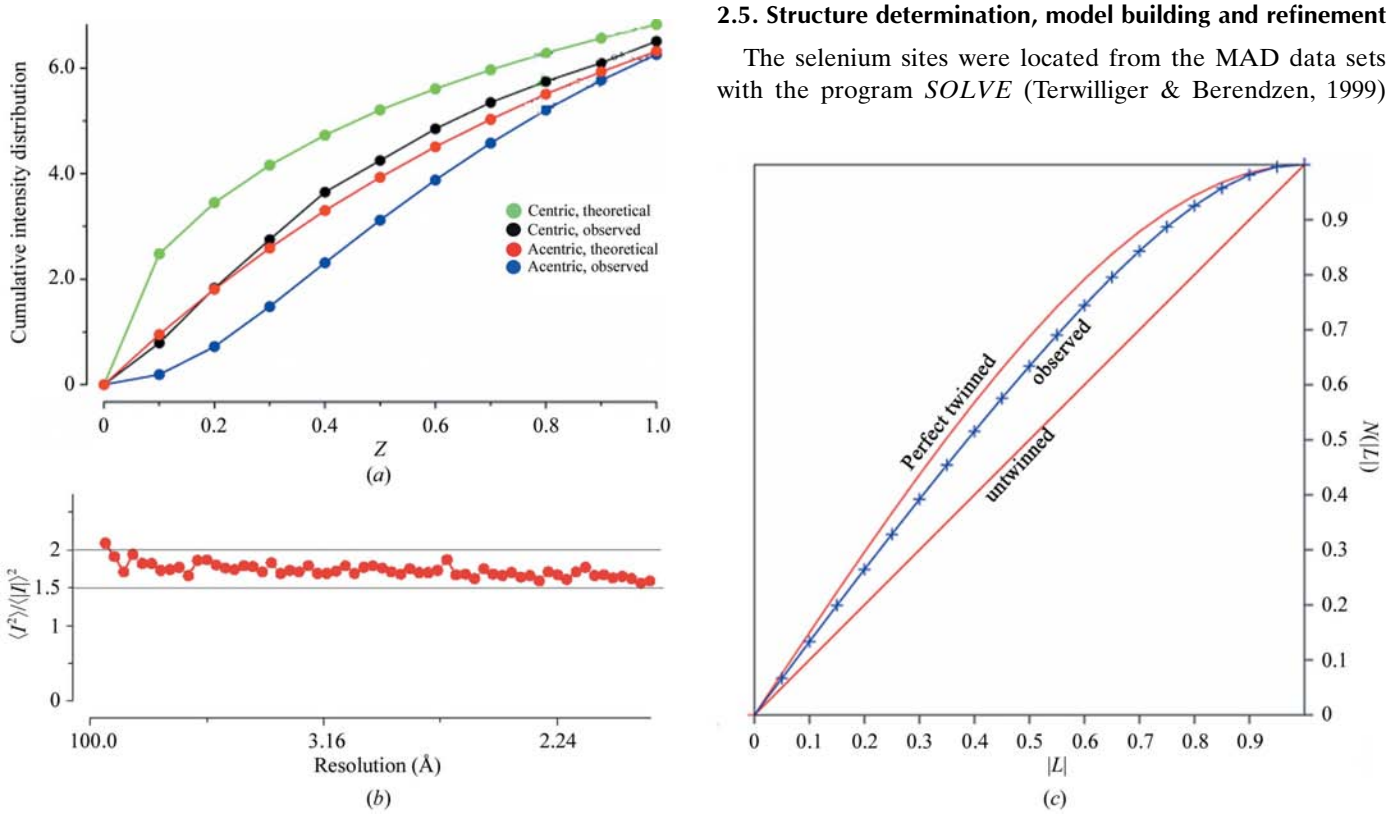

Figure 2
Twin pathology. The figures were derived using the 2.0 Å data set from a native AknOx crystal. (*a*) Cumulative intensity distributions of $Z = I/\langle I\rangle$, where I is the intensity of centric and acentric reflections. (*b*) The second intensity moment ($\langle I^2\rangle/\langle|I|\rangle^2$) calculated for the acentric data. (*c*) The local intensity distribution curve, $N(|L|)$ *versus* $|L|$. The experimental curve for the observed AknOx data falls between the curves expected for untwinned and perfectly twinned data.

using the MAD protocol and diffraction data to 3 Å resolution. Subsequently, the phases from *SOLVE* were improved by the density-modification program *RESOLVE* (Terwilliger, 2000). The phases were then extended to 2.7 Å using the peak data set only with the program *DM* (Collaborative Computational Project, Number 4, 1994). The auto-build option of the program *PHENIX* (Adams *et al.*, 2004) was used to trace the polypeptide chains from the electron-density map calculated to 2.7 Å resolution. The resulting model was completed manually and the amino-acid sequence was fitted to the electron-density map using *Coot* (Emsley & Cowtan, 2004). Phase combination was carried out by sequentially using *SFTOOLS*, *CAD* and *SIGMAA* from the *CCP*4 interface (Collaborative Computational Project, Number 4, 1994). The combined phases were then used in *FFT* (Collaborative Computational Project, Number 4, 1994) to create the electron-density map. Several rounds of phase combination and model building led to a complete model of the four molecules of AknOx in the asymmetric unit and this model was then used for further refinement.

The crystallographic refinement was performed with *SHELXL* (Sheldrick & Schneider, 1997) using the twinning protocol, noncrystallographic symmetry (NCS) restraints and isotropic *B* factors. Initially, refinement was carried out using the native 2.0 Å data set and was then continued with the high-resolution data set to 1.65 Å. Most of the structure was included in the NCS restraints except for a loop region consisting of residues 259–264 and a few residues which had differences in their side-chain conformations in different monomers. A total of 4% of the reflections were excluded from the refinement as the test set, chosen in thin shells as recommended for twin refinement. Water molecules were

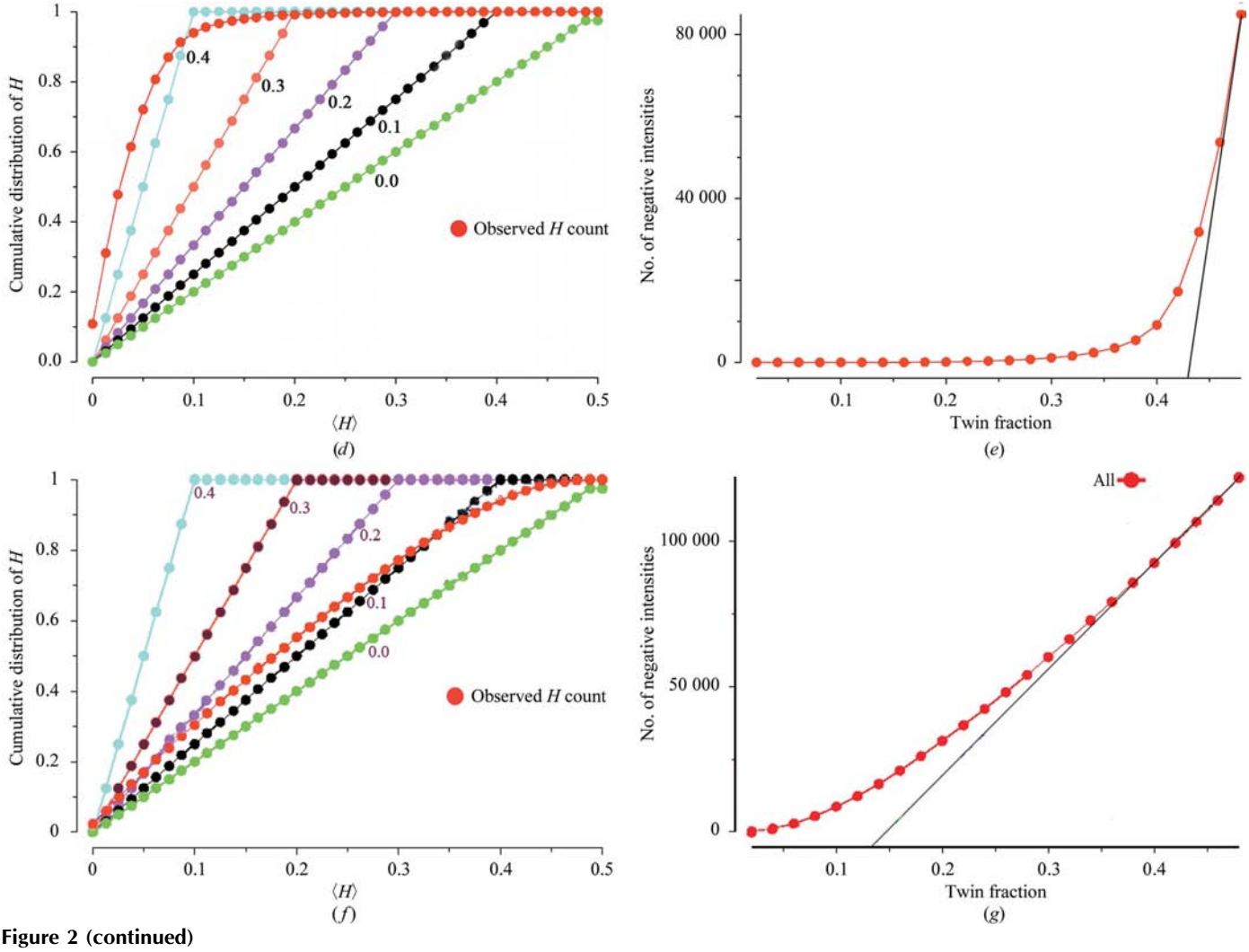

Figure 2 (continued)
(*d*) Estimation of the twin fraction from the cumulative distribution of H by using the two-domain ($a = c$) twin operator $l, -k, h$ for two-domain twinning. (*e*) Twin fraction from the Britton plot using the two-domain operator $l, -k, h$. (*f*) Estimation of the twin fraction, α, by plotting the fractional intensity difference between acentric twin-related intensities. The initial slope of the distribution is a measure of α. Expected slopes for given twin fractions are shown for comparison. The red line represents the slope for the experimental data. The plot was calculated using one of the twin operators, $l, k, -h - l$, for three-domain twinning. (*g*) Estimation of the twin fraction from a Britton plot. After detwinning, the number of negative intensities is plotted as a function of the assumed value of α. An overestimation of α will lead to an increased number of negative intensities and the actual value of α is estimated from this increase. The line is only fitted linearly to the data when the twin fraction is larger than 0.14. The plot was calculated using one of the twin operators, $l, k, -h - l$, for three-domain twinning.

manually added to the model based on $F_o - F_c$ electron-density maps using *Coot*. The stereochemistry of the final model was analyzed by *PROCHECK* from the *CCP*4 program suite.

The molecular images were prepared using *PyMOL* (DeLano, 2002).

3. Results and discussion

3.1. Space-group determination and detection of twinning

The first native AknOx data set was collected to 2.0 Å resolution. Data processing with *XDS* suggested a primitive monoclinic unit cell, with unit-cell parameters a = 68.2, b = 264.5, c = 68.2 Å, β = 118.7°. Merging of the data in space group $P2_1$ (the exact assignment was based on systematic absences along 0k0) gave an overall R_{sym} of 0.052 with $I/\sigma(I)$ = 19.4 (Table 1). The data could also be processed in the trigonal space group $P3$; however, merging of these data resulted in an R_{sym} of 0.44, suggesting that $P3$ is not the true space group of the AknOx crystals. The data set could also be indexed and scaled with an R_{sym} of 0.072 in the orthorhombic space group $C222_1$ (unit-cell parameters a = 69.7, b = 117.5, c = 264.4 Å). However, the intensity statistics and distributions indicated severe twinning, which is not consistent with the orthorhombic cell as the space group of the AknOx crystals. Inspection of the Harker sections of the anomalous difference Patterson map calculated from the selenomethionine data in the orthorhombic space group did not show any significant peaks, which again excluded $C222_1$ as the correct space group.

The first indications of twinning in the native 2.0 Å data set were the low values of the second moment ($\langle I^2\rangle/2\langle I\rangle^2$) = 0.845 calculated by *XDS* (compared with 1.0 for an untwinned crystal; Kabsch, 1993). The presence of twinning was further suggested by the cumulative intensity distribution, $N(Z)$, and analysis of the second moment of intensities of the acentric data $\langle I^2\rangle/\langle|I|\rangle^2$ (Yeates, 1997; Stanley, 1972). The cumulative intensity-distribution plot (Stanley, 1972; Rees, 1980; Dauter, 2003) for both centric and acentric reflections showed a sigmoidal shape compared with the expected distribution for untwinned data (Fig. 2*a*). As previously observed during data processing, the expected values for the second intensity moment ($\langle I^2\rangle/\langle|I|\rangle^2$) are 2.0 and 1.5 for an untwinned and a perfectly twinned case, respectively, and the value of 1.66 for acentric reflections in the AknOx data set (Fig. 2*b*) clearly indicated the presence of twinning. A related parameter, $\langle|F|\rangle^2/\langle F^2\rangle$, which should be 0.785 for untwinned and 0.865 for perfectly twinned data, was calculated using *CNS* (Brünger *et al.*, 1998). The value of 0.857 for the AknOx data also indicated the presence of twinning. A more recent test for the detection of twinning based on local intensity differences, which is less sensitive to anisotropy and pseudo-centring, has been implemented by Padilla & Yeates (2003). The cumulative probability distribution $N(|L|)$ *versus* $|L|$, where L is defined as $[I(\mathbf{h}_1) - I(\mathbf{h}_2)]/[I(\mathbf{h}_1) + I(\mathbf{h}_2)]$ and $I(\mathbf{h}_1)$ and $I(\mathbf{h}_2)$ are the intensities of the unrelated reflections $\mathbf{h}_1$ and $\mathbf{h}_2$ indeed also gave a clear sign of twinning (Fig. 2*c*). The observed values of $\langle|L|\rangle$ and $\langle L^2\rangle$ were 0.405 and 0.228, respectively, compared with the theoretical values for acentric perfectly twinned data (0.375 and 0.2, respectively) and those for acentric nontwinned data (0.5 and 0.333, respectively).

In order to estimate the twinning fraction(s), a test for partial twinning using the cumulative intensity distribution of H (Yeates, 1988), where $H = |I_{obs1} - I_{obs2}|/|I_{obs1} + I_{obs2}|$, was performed. For a monoclinic lattice with unit-cell parameters $a = c$ and β close to 120°, several possibilities exist that will result in pseudomerohedrally twinned crystals. The two equal cell edges ($a = c$) can allow a twinning operator l, $-k$, h, *i.e.* a twofold rotation about the axis diagonal between the monoclinic a and c directions (Yang *et al.*, 2000). Using this operator in both the H-test and Britton plot (Fisher & Sweet, 1980) the twin fraction was estimated to 0.43 (Figs. 2*d* and 2*e*), which was later refined to the value of 0.50 in *SHELXL* (Sheldrick & Schneider, 1997). This high twin fraction is consistent with the similar R_{sym} values obtained from scaling the data in $P2_1$ and $C222_1$. A monoclinic lattice with $a = c$ and β close to 120° can emulate a hexagonal metric. Such twins are known from small-molecule crystallography and contain three twin domains (Langer *et al.*, 2004). In the case of AknOx, the three domains would be related by identity, h, k, l, and two threefold rotations $-h - l$, k, h and l, k, $-h - l$. Estimates of the twin fractions using the twin operators l, k, $-h - l$ (Fig. 2*f*) and $-h - l$, k, h, respectively, for three-domain twinning one at a time gave values for α_1 and α_2 of 0.13, which was in good agreement with the values of 0.14 estimated from the Britton plot (Fig. 2*g*). It is noteworthy that the two twinning fractions (α_1 and α_2) obtained from *SHELXL* during refinement with the 2 Å resolution data set using the three-domain twin protocol had equal values of 0.14 (see below).

The native high-resolution data set (1.65 Å) and the three data sets from the selenomethionine-substituted crystals were also processed in the monoclinic space group $P2_1$ with almost identical unit-cell parameters (Table 1). Analysis of these data sets using the same protocols as above resulted in the same indications of pseudomerohedral twinning for all cases.

The results of the analysis of the intensity statistics of the AknOx data all indicated that these crystals were pseudomerohedrally twinned. However, at this stage of the analysis the assignment of the twin laws giving rise to the twinning of the AknOx crystals could not be established unambiguously

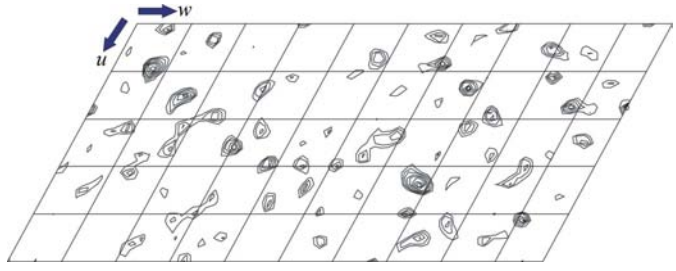

Figure 3
Harker section of the anomalous difference Patterson map calculated in $P2_1$, contoured at 1.5σ.

and had to await the analysis of crystal packing and refinement of the structure as described in the following sections.

3.2. Structure determination

The content of the asymmetric unit was estimated from the Matthews coefficient (Matthews, 1968), which suggested a value of 2.37 Å^3 Da^{-1} with 48% solvent content corresponding to four molecules per asymmetric unit (ASU). The Harker section of the anomalous difference Patterson map calculated in $P2_1$ showed a number of peaks corresponding to the Se atoms in the crystals (Fig. 3). The three data sets collected from the selenomethionine-substituted crystal were used for phasing by MAD. The program *SOLVE* (Terwilliger & Berendzen, 1999) found all 24 expected selenium sites from the four molecules in the ASU, with a figure of merit of 0.50 to 3.0 Å resolution. The phases were then improved by density modification including NCS averaging (the NCS operators were derived from the positions of the selenium sites using *RESOLVE*) and solvent flattening. The resolution was then extended to 2.7 Å using the peak data set. In the course of the structure determination by MAD, the twinned selenomethionine data sets were used and no detwinning procedures were employed. In a MAD experiment, small differences in the intensities must be measured and can be expected to be swamped by the averaging effect of twinning. Nevertheless, several MAD structures have been reported from hemihedrally (Dauter, 2003; Yang *et al.*, 2000; Rudolph *et al.*, 2003; Larsen & Harrison, 2004; Toms *et al.*, 2004) and tetartohedrally (Barends *et al.*, 2005) twinned protein crystals using twinned data. In the case of AknOx, the overall quality of the map obtained directly after density modification in *RESOLVE* (Terwilliger, 2000) very clearly showed the secondary-structure features including density for β-sheets and α-helices (Fig. 4*a*). With the exception of several loop regions, a complete model of the structure of AknOx could be built from the experimental MAD electron-density map using the twinned data.

3.3. Model building and phase combination

In the initial stage of model building, the experimental map was used for automated model building with the program *PHENIX* (Adams *et al.*, 2004). Parts of the β-sheets as well as several α-helices were built automatically by the program as a polyalanine model consisting of approximately 1200 of the total of 2008 amino-acid residues for all four molecules in the ASU. Model building was then continued manually by extending the polypeptide model and by incorporating the correct sequence, guided by the selenium sites. At the end of this stage, most of the secondary-structure elements had been built except for 50–55 residues in each monomer which mainly belonged to the loop regions of the structure. Phase combination alternated with manual model building was used to improve the electron-density map and to build the missing parts of the model. After the first cycle of phase combination, model building of most of the missing or less well defined loops of the protein molecules (Figs. 4*b* and 4*c*), as well as placement of the cofactor, FAD, and the bound ligand, AclA, was rather straightforward. The present model of AknOx consists of 492 of a total of 502 amino acids (*i.e.* 1968 of 2008 amino-acid residues in the ASU) and 1009 water molecules, including FAD bound in all four molecules in the ASU and the ligand AclA bound in one molecule of AknOx. The missing parts in each molecule include the His tag as well as the first nine residues and the C-terminal residue of the polypeptide chain.

3.4. Refinement against the twinned data

Refinement of the structure with no twinning stalled at unacceptably high R factors ($R_{\rm free}$ = 35%; here and in the following R factors are calculated on all data; no sigma cutoff was applied), again indicating that the AknOx crystals are pseudomerohedrally twinned. In order to cross-validate the refinement in a correct way for twinned data, it is necessary to select the set of test reflections in such a way that any reflection and its twin-related reflections would all be either in the

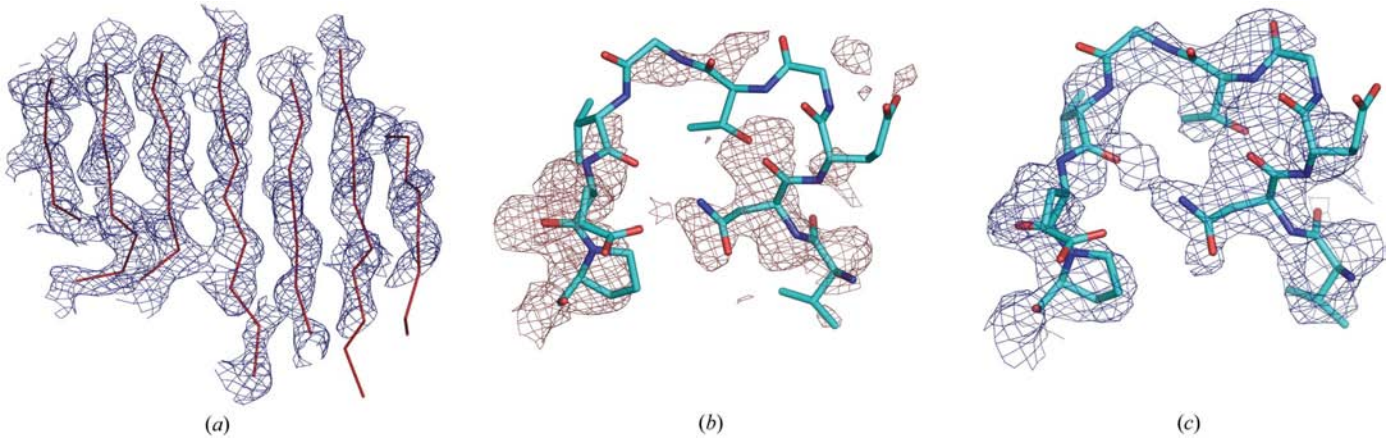

Figure 4
MAD-phased electron-density map and phase combination. (*a*) The MAD-derived electron-density map after density modification in *RESOLVE* calculated to 3.0 Å resolution and contoured at 1.0σ. Parts of the initial model (only the C$^\alpha$ trace is shown for better clarity), built by the program *PHENIX*, are shown in red. (*b*, *c*) Electron-density map for one of the missing loops (residues 309–315) before (*b*) and after (*c*) the first round of phase combination. The final refined model is included.

test set or in the reference set used for refinement (Barends *et al.*, 2005). For the AknOx data set, the test reflections were selected using *SHELXPRO* (Sheldrick, 1990) in thin resolution shells, as recommended for twin refinement. The refinement program *SHELXL* (Sheldrick & Schneider, 1997) was used throughout refinement.

At the outset of the refinement, we had to decide which twin operators should be used. Test runs with the initial protein model, the 2.0 Å native data set and the twinning operator $l, -k, h$ (TWIN 0 0 1 0 −1 0 1 0 0 in *SHELXL*; two-domain twinning) gave a large difference between $R_{\rm fac}$ (27%) and $R_{\rm free}$ (39%). The same model, but including three-component twinning with the twinning operator $l, k, -h - l$ (TWIN 0 0 1 0 1 0 −1 0 −1 in *SHELXL*) and two values for the twin fraction, resulted in a lower $R_{\rm free}$ (35%) and a difference between $R_{\rm fac}$ and $R_{\rm free}$ of only 3%, indicating a better behaved refinement process. The refinement was therefore continued using the three-domain twinning protocol. Tight NCS restraints were applied to partially compensate for the low observation-to-parameter ratio caused by the three-domain twinning. Refinement, interspersed with manual model building using the native twinned 2 Å data set, was carried to an $R_{\rm free}$ value of about 27% (with no waters added). At this stage, a high-resolution data set (1.65 Å) became available and was used for further refinement. *SHELXL* allows the refinement of the twin fractions α_1 and α_2. These were 0.14 and 0.14 for the 2 Å resolution data set and 0.16 and 0.16 for the high-resolution data set. It is noteworthy that these values are in agreement with the estimates of twin fractions using other methods (see above). The refinement of the model resulted in an $R_{\rm free}$ of 26.5% and an $R_{\rm fac}$ of 23.1%. However, in the case of twin refinement, the data-to-parameter ratio is significantly lower compared with untwinned data, mostly because of the averaging of twin-related reflections (Rudolph *et al.*, 2004; Barends *et al.*, 2005). Therefore, $R_{\rm free}$ values for refined protein structures from twinned crystals could be higher than those obtained from refinement against data from untwinned crystals.

At this stage, the question of two-domain twinning was revisited and the final model obtained from the three-domain twin refinement was used for further refinement by the two-domain twin protocol (twin operator $l, -k, h$) using the same set of test reflections as for three-domain twinning. The refinement procedure led to an $R_{\rm fac}$ and $R_{\rm free}$ of 18.5 and 24.2%, respectively, with a refined twin fraction of 0.505.

The refinement of the AknOx model, using two different types of pseudomerohedral twinning, led in both cases to comparable $R_{\rm free}$ values and model statistics and both procedures thus describe the data almost equally well. The perfect two-domain twinning appears to be a better model of the twinning of the AknOx crystals because it is consistent with the orthorhombic metric of the lattice as indicated by the low $R_{\rm sym}$ of the data scaled in $C222_1$ and also leads to a lower $R_{\rm free}$. However, the lower $R_{\rm free}$ may also reflect a better confidence

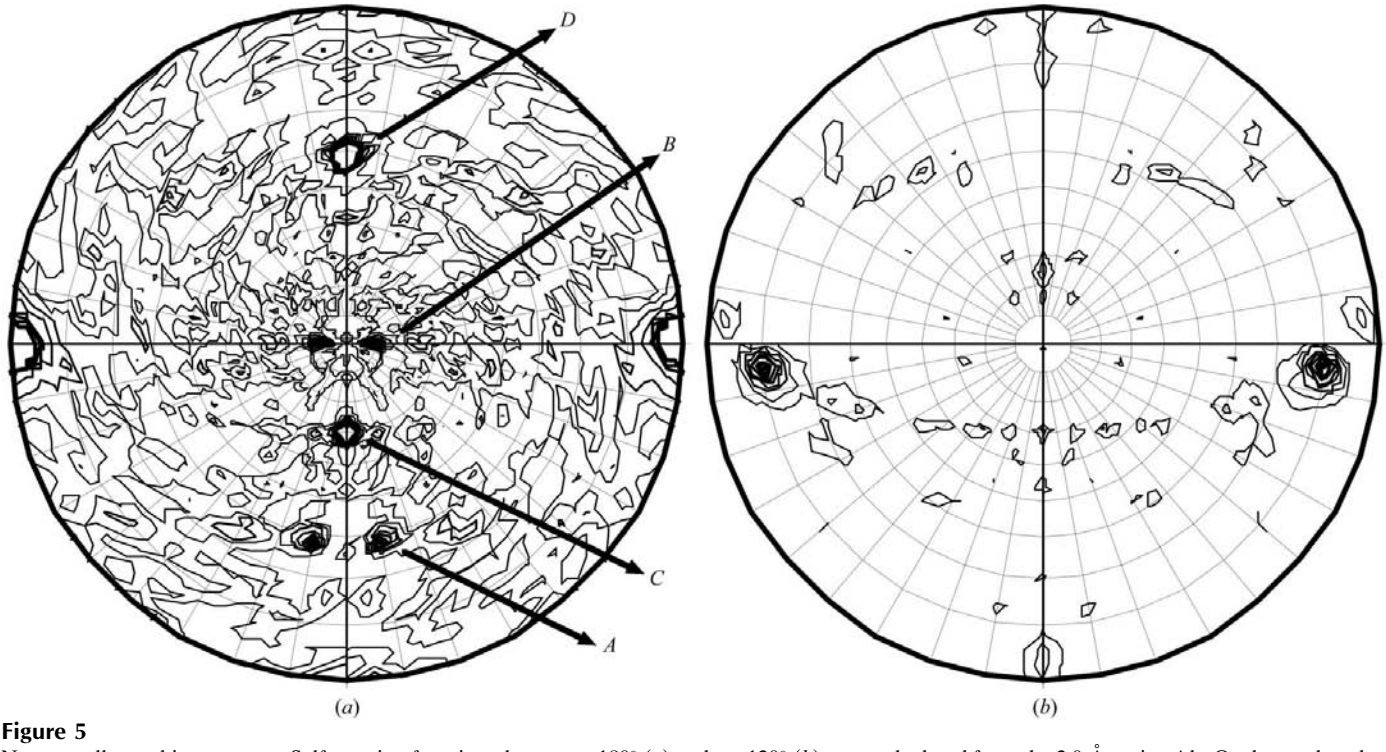

Figure 5
Noncrystallographic symmetry. Self-rotation function plots at $\kappa = 180^\circ$ (*a*) and $\kappa = 120^\circ$ (*b*) were calculated from the 2.0 Å native AknOx data reduced to space group $P2_1$. The twofold NCS peaks labelled *A* and *B* (peak heights 7.0 and 6.0, respectively) are generated by the molecular twofolds passing through the dimers *AB* and *CD*, respectively. The third twofold NCS axis, labelled *C* (peak height 27.6), relates the two dimers *AB* and *CD* in the asymmetric unit. The twofold NCS axis *D* (peak height 27.6) is generated by the combination of the crystallographic 2_1 axis and the NCS axis *C*. The peak at $\kappa = 120^\circ$ is caused by the incomplete threefold packing in the crystal. The height of this pseudo-threefold peak (6.5) is approximately five times lower than that of the crystallographic twofold axis (30.8). The $\kappa = 60^\circ$ section does not contain any peaks above the noise level.

in the estimation of the individual intensities in the case of two-domain *versus* three-domain twinning. Taken together, these findings point towards the possibility that the AknOx crystals show sixfold pseudomerohedral twinning, a dyad along the diagonal between the *a* and *c* axes and a threefold twinning operator almost parallel to the monoclinic *b* axis, giving six twin domains in these crystals. Such multidomain crystals have been described for small-molecule crystals (Friese *et al.*, 2003). Unfortunately, none of the presently available refinement programs can handle this type of multi-domain twinning in protein crystals.

3.5. Crystal packing and cause of twinning

A self-rotation function was calculated from the 2.0 Å data set reduced to space group $P2_1$. The plot of the $\kappa = 180^\circ$ section showed four NCS axes perpendicular or almost perpendicular to the crystallographic *b* axis (Fig. 5). The four subunits (denoted *A*–*D*) in the asymmetric unit of the crystal are packed as two dimers (Fig. 6) and the NCS peaks denoted *A* and *B* in Fig. 4(*a*) are generated by the molecular twofolds of the dimers *AB* and *CD*, respectively. The NCS peak *C* reflects a twofold axis that relates the *AB* and *CD* dimers in the ASU (Fig. 6). Peak *D* is generated by the combination of the crystallographic twofold screw axis perpendicular to the twofold NCS axis *C*. A self-rotation function calculated from structure-factor amplitudes derived from the refined AknOx model reproduces the self-rotation function obtained from experimental data. The twofold twin operator in AknOx, located on a diagonal between the monoclinic *a* and *c* axes, is parallel to the twofold NCS axis relating the two dimers in the asymmetric unit and thus overlaps with peaks *C* and *D* in the rotation function.

The peak observed at $\kappa = 120^\circ$ (Fig. 5) is positioned almost parallel to the crystallographic *b* axis. This peak is generated by an unusual asymmetric trimer packing in the crystals of AknOx. An investigation of the molecular packing revealed that the dimers *AB* and *CD* are related by a rotation of almost 120° and a translation of approximately one-third of the unit cell nearly parallel to the *b* axis (Fig. 6). The peak in the $\kappa = 120^\circ$ section of the self-rotation function is thus the result of the pseudo-trimer screw axis which is generated by the formation of two-thirds of the trimer in the cell. The gap in the pseudo-trimer is filled by a symmetry partner of one of the

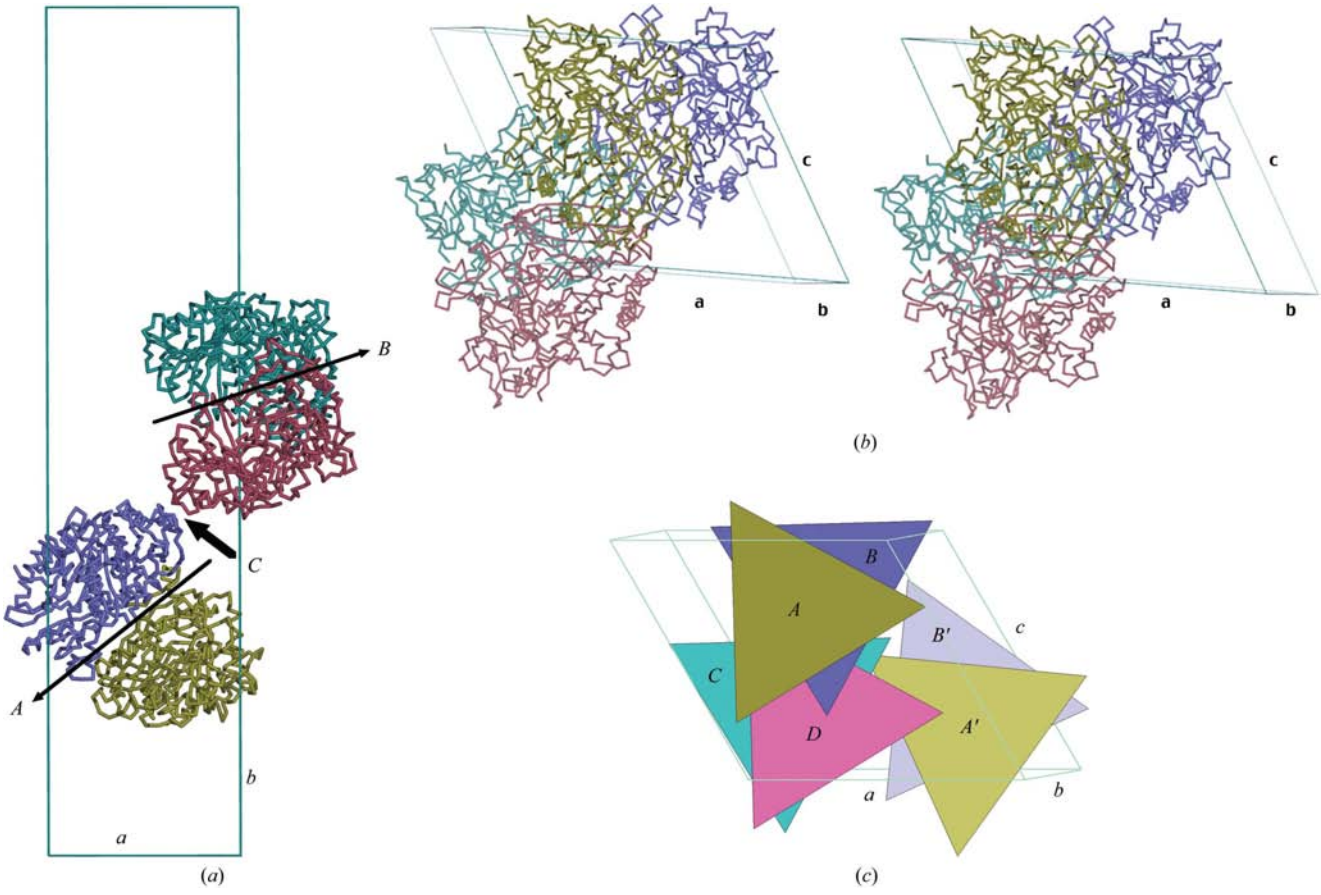

Figure 6
Molecular packing. (*a*, *b*) Perpendicular views of the packing of AknOx in the crystal asymmetric unit. Dimer *AB* (olive and blue, respectively) is related to dimer *CD* (cyan and pink, respectively) by a 120° rotation and a translation by approximately one-third of the unit cell. The three arrows labelled *A*, *B* and *C* indicate the three twofold NCS axes as in Fig. 4. (*c*) Schematic view of the pseudo-trimeric packing in the unit cell. The third dimer (*A*′*B*′) which breaks the threefold symmetry is depicted in light colours. This dimer is related to dimer *AB* by the crystallographic 2_1 symmetry. Otherwise, the colouring follows that of (*a*) and (*b*). The cell axes *a*, *b* and *c* are labelled.

participating dimers, related by the crystallographic 2_1 symmetry shift along the *b* axis (Fig. 6*c*). A similar but not identical unusual 'pseudo-trimer' symmetry has recently been found in crystals of the enzyme PFL2 from *Archeoglobus fulgidus* (Lehtiö *et al.*, 2006).

The incomplete threefold packing can also be seen as the main reason for the three-domain (or possibly six-domain) twinning in the AknOx crystals. The dimers in the ASU can pack in three different combinations by altering their relative position in this pseudo-trimer packing (Figs. 7*a* and 7*b*). The NCS and the twinning operators coincide along the same axis almost parallel to the crystallographic *b* axis. Consequently, the peaks in the $\kappa = 120^\circ$ section of the self-rotation function reflecting the pseudo-trimer axis and the three-domain twinning overlap. The pseudomerohedral twinning in the crystals of AknOx would thus arise from the fact that the NCS and twin operators are (almost) parallel, a situation which also has been observed in a number of other cases of pseudomerohedrally twinned crystals (Barends & Dijkstra, 2003; Declercq & Evrard, 2001; Frazao *et al.*, 1999).

4. Conclusions

In this paper, we have described the structure determination and refinement of AknOx from pseudomerohedrally twinned crystals. The presence of twinning in the crystal was confirmed by several twinning tests using intensity statistics and the twinning fraction was initially estimated by different methods such as the *H*-test and Britton plot and finally refined during the structure refinement. Packing considerations and refinement are consistent with perfect pseudomerohedral two-domain twinning with the twin operator being a twofold rotation along the diagonal between the *a* and *c* axes of the monoclinic lattice. On the other hand, the unit cell with two

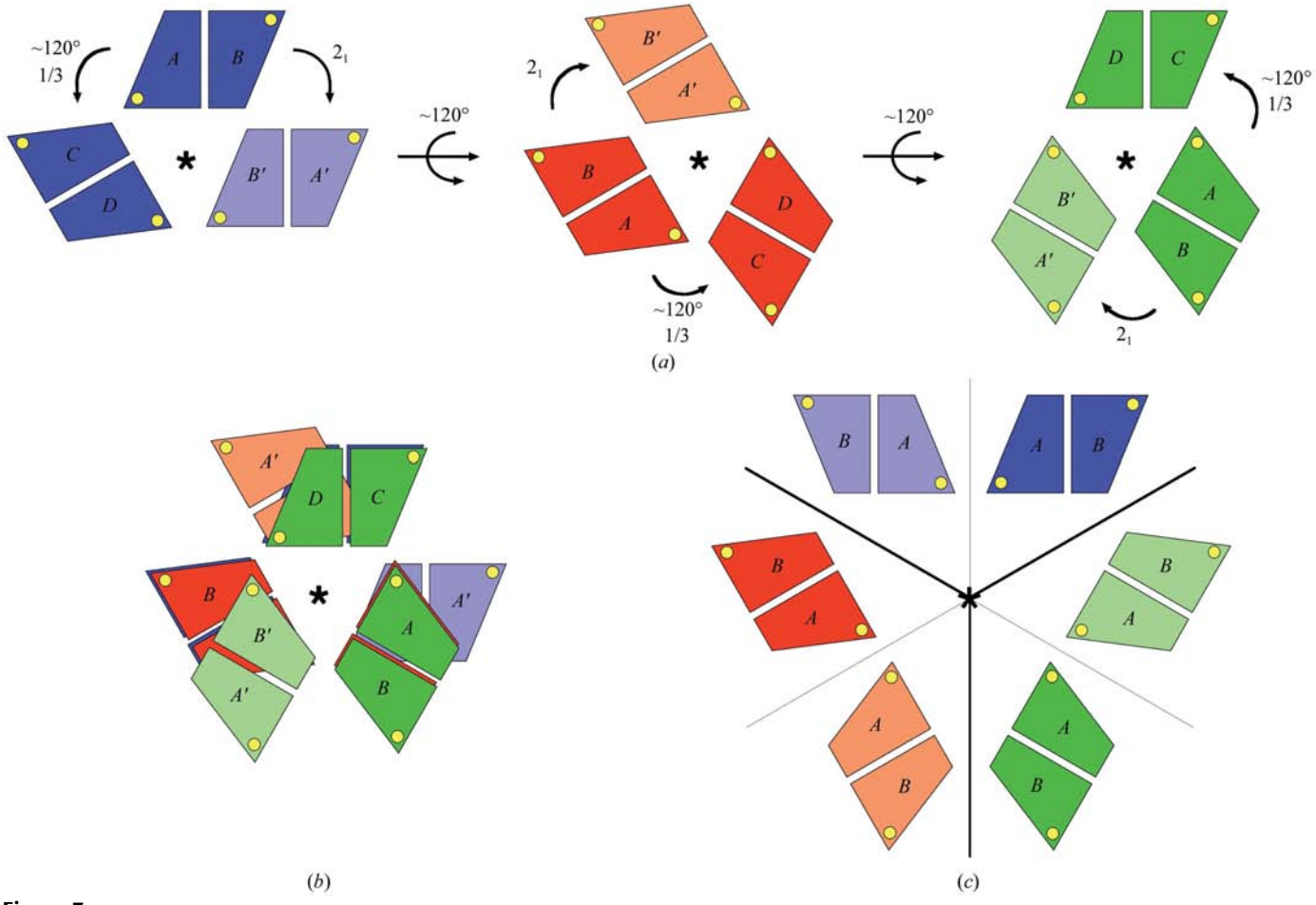

Figure 7
Molecular packing and twinning. The three twin domains of the putative *Drilling* are shown in blue, red and green. The asterisk indicates the pseudo-threefold axis almost parallel to the crystallographic *b* axis. The threefold twin operator coincides with this pseudo-threefold NCS axis. (*a*) In each twin domain, two dimers are related by a rotation of approximately 120° and a translation of roughly 1/3. The third partner of this asymmetric trimer is generated by crystallographic symmetry (indicated by 2_1; see also Fig. 6*c*). (*b*) Superposition of the three twin domains on top of each other. In this view, it is evident that the 120° rotated dimer pairs superimpose perfectly in the three twin domains, whereas the crystallographic 2_1 mate does not. (*c*) Illustration of the possible combination of two-domain and three-domain twinning in crystals of AknOx. The thick black lines indicate the interconverting *a* and *c* axes in the two-domain twin cells and the two-domain twin pairs are coloured in dark and light shades of the same colour. The location of the twofold twin operator in each of the three *Drilling* domains is indicated by the thin black line equally distant from the *a* and *c* axes. Note that the six individual twin domains generated by the combination of threefold and two-old twin operators perpendicular to each other are not related by sixfold symmetry.

nearly equal unit-cell axes ($a = c$) and a β angle of approximately 120° suggested the presence of three-domain twinning within the monoclinic cell. A pseudo-threefold NCS axis exactly parallel to the twin axis as observed in the AknOx crystals would promote this type of twinning. The final model could also be refined to a similar $R_{\rm free}$ using this three-domain twin operator. The slightly lower $R_{\rm free}$ obtained using the twofold twin operator could at least partially be explained by a higher confidence in the estimation of the individual intensities in the case of two-domain *versus* three-domain twinning. The fact that the structure of AknOx can be refined with comparable R values using either of the twin operators separately, but the $R_{\rm free}$ in both cases remains rather high, points to the possibility that both models describe the approximation of the real situation but not in a sufficient way. This raises the possibility that the crystals of AknOx are built of several twin domains related by a combination of two twinning operators, *i.e.* a twofold twinning operator along the diagonal between *a* and *c* and threefold twinning almost parallel to the monoclinic *b* axis, resulting in six twin domains (Fig. 7*c*). This type of twinning has been described in small-molecule crystallography (Friese *et al.*, 2003). At present, it is not possible to refine the data from protein crystals using both twin operators and the presence of multiple twinning in AknOx thus cannot be proven conclusively.

We gratefully acknowledge access to synchrotron radiation at the EMBL Outstation, DESY, Hamburg, MAX Laboratory, Lund, Sweden and the ESRF, Grenoble, France. IK acknowledges a Marie Curie Intra-European Fellowship. This work was supported by the Swedish Research Council and the Academy of Finland (grant No. 210576).

References

Adams, P. D., Gopal, K., Grosse-Kunstleve, R. W., Hung, L. W., Ioerger, T. R., McCoy, A. J., Moriarty, N. W., Pai, R. K., Read, R. J., Romo, T. D., Sacchettini, J. C., Sauter, N. K., Storoni, L. C. & Terwilliger, T. C. (2004). *J. Synchrotron Rad.* **11**, 53–55.

Ban, N., Nissen, P., Hansen, J., Capel, M., Moore, P. B. & Steitz, T. A. (1999). *Nature (London)*, **400**, 841–847.

Barends, T. R., de Jong, R. M., van Straaten, K. E., Thunnissen, A. M. & Dijkstra, B. W. (2005). *Acta Cryst.* D**61**, 613–621.

Barends, T. R. & Dijkstra, B. W. (2003). *Acta Cryst.* D**59**, 2237–2241.

Brünger, A. T., Adams, P. D., Clore, G. M., DeLano, W. L., Gros, P., Grosse-Kunstleve, R. W., Jiang, J.-S., Kuszewski, J., Nilges, M., Pannu, N. S., Read, R. J., Rice, L. M., Simonson, T. & Warren, G. L. (1998). *Acta Cryst.* D**54**, 905–921.

Chandra, N., Acharya, K. R. & Moody, P. C. (1999). *Acta Cryst.* D**55**, 1750–1758.

Collaborative Computational Project, Number 4 (1994). *Acta Cryst.* D**50**, 760–763.

Dauter, Z. (2003). *Acta Cryst.* D**59**, 2004–2016.

Declercq, J. P. & Evrard, C. (2001). *Acta Cryst.* D**57**, 1829–1835.

DeLano, W. L. (2002). *The PyMOL Molecular Graphics System.* DeLano Scientific, San Carlos, CA, USA. http://www.pymol.org

Emsley, P. & Cowtan, K. (2004). *Acta Cryst.* D**60**, 2126–2132.

Fisher, R. G. & Sweet, R. M. (1980). *Acta Cryst.* A**36**, 755–760.

Frazão, C., Sieker, L., Coelho, R., Morais, J., Pacheco, I., Chen, L., LeGall, J., Dauter, Z., Wilson, K. & Carrondo, M. A. (1999). *Acta Cryst.* D**55**, 1465–1467.

Friese, K., Kienle, L., Duppel, V., Luo, H. & Lin, C. (2003). *Acta Cryst.* B**59**, 182–189.

Ito, N., Komiyama, N. H. & Fermi, G. (1995). *J. Mol. Biol.* **250**, 648–658.

Kabsch, W. (1993). *J. Appl. Cryst.* **26**, 795–800.

Kleywegt, G. J. & Jones, T. A. (1996). *Acta Cryst.* D**52**, 826–828.

Kallio, P., Sultana, A., Niemi, J., Mäntsälä, P. & Schneider, G. (2006). *J. Mol. Biol.* **357**, 210–20.

Kursula, P. (2004). *J. Appl. Cryst.* **37**, 347–348.

Langer, V., Smrcok, L. & Masuda, Y. (2004). *Acta Cryst.* C**60**, i104–i106.

Larsen, N. A. & Harrison, S. C. (2004). *J. Mol. Biol.* **344**, 885–892.

Larsen, N. A., Heine, A., de Prada, P., Redwan, E.-R., Yeates, T. O., Landry, D. W. & Wilson, I. A. (2002). *Acta Cryst.* D**58**, 2055–2059.

Lehtiö, L., Grossmann, J. G., Kokona, B., Fairman, R. & Goldman, A. (2006). *J. Mol. Biol.* **357**, 221–235.

Liang, J., Ealick, S., Nielsen, C., Schreiber, S. L. & Clardy, J. (1996). *Acta Cryst.* D**52**, 207–210.

Lietzke, S. E., Carperos, V. E. & Kundrot, C. E. (1996). *Acta Cryst.* D**52**, 687–692.

Matthews, B. W. (1968). *J. Mol. Biol.* **33**, 491–497.

Padilla, J. E. & Yeates, T. O. (2003). *Acta Cryst.* D**59**, 1124–1130.

Räty, K., Kantola, J., Hautala, A., Hakala, J., Ylihonko, K. & Mäntsälä, P. (2002). *Gene*, **293**, 115–122.

Rees, D. C. (1980). *Acta Cryst.* A**36**, 578–581.

Rudolph, M. G., Kelker, M. S., Schneider, T. R., Yeates, T. O., Oseroff, V., Heidary, D. K., Jennings, P. A. & Wilson, I. A. (2003). *Acta Cryst.* D**59**, 290–298.

Rudolph, M. G., Wingren, C., Crowley, M. P., Chien, Y. H. & Wilson, I. A. (2004). *Acta Cryst.* D**60**, 656–664.

Schneider, G. (2005). *Curr. Opin. Struct. Biol.* **15**, 629–636.

Sheldrick, G. M. (1990). *Acta Cryst.* A**46**, 467–473.

Sheldrick, G. M. (1997). *The SHELX-97 Manual*, ch. 6.4, pp. 43–44. http://shelx.uni-ac.gwdg.de/SHELX/

Sheldrick, G. M. & Schneider, T. R. (1997). *Methods Enzymol.* **277**, 319–343.

Stanley, E. (1972). *J. Appl. Cryst.* **5**, 191–194.

Terwilliger, T. C. (2000). *Acta Cryst.* D**56**, 965–972.

Terwilliger, T. C. & Berendzen, J. (1999). *Acta Cryst.* D**55**, 849–861.

Toms, A. V., Kinsland, C., McCloskey, D. E., Pegg, A. E. & Ealick, S. E. (2004). *J. Biol. Chem.* **279**, 33837–33846.

Vagin, A. & Teplyakov, A. (1997). *J. Appl. Cryst.* **30**, 1022–1025.

Yang, F., Dauter, Z. & Wlodawer, A. (2000). *Acta Cryst.* D**56**, 959–964.

Yeates, T. O. (1988). *Acta Cryst.* A**44**, 142–144.

Yeates, T. O. (1997). *Methods Enzymol.* **276**, 344–358.

Yeates, T. O. & Fam, B.-C. (1999). *Structure*, **7**, R25–R29.